A model-based comparison of Ru and Ni catalysts for the Sabatier reaction

Emanuele Moioli[a,b], Andreas Züttel[a,b]

[a]Laboratory of Materials for Renewable Energy, Institute of Chemical Sciences and Engineering, École Polytechnique Fédérale de Lausanne (EPFL), 1950 Sion, Switzerland

[b]Swiss Federal Laboratories for Materials Science and Technology (EMPA), 8600 Dübendorf, Switzerland

Abstract

The differences between Ru- and Ni-based catalysts for the Sabatier reactor are assessed on the basis of appropriate kinetic models and reactor designs. The origin of the higher performance of the Ru-based catalyst is analysed in detail. Ru activates the reactor and initiates the thermal runaway at about 100°C lower than commercial Ni/Mg/Al_2O_3 catalysts and 10-20 °C lower than new Ni/Al_2O_3 catalysts. In addition, the higher catalytic activity at the low temperature of Ru-based catalysts allows the thermodynamic curve to be followed-up to the region of high CO_2 conversion. Over steam reforming Ni catalysts, the highest attainable conversion is instead limited to 90%, while tailored Ni catalysts for CO_2 methanation can reach 96% conversion in a single pass reactor. In the intermediate conversion areas, the two catalysts show comparable activity, due to the reaction limitations which are related to the required cooling and to the diffusional limitations that are more pronounced in the highly active Ru. We developed a reactor design to define the amount of catalyst required to reach grid-compatible CO_2 conversion, and found that 99.5% conversion is attainable in a single step with a 0.5% Ru/Al_2O_3 catalyst or with a high load of Ni/Al_2O_3 by introducing an intermediate water condensation step. As a consequence, we calculated that the cost of the catalyst is approximately two to three times higher for the Ru-based reactor than the Ni-based. However, this difference in catalyst cost cannot compensate for the cost of a more complex system, including several different units, when developing energy storage solutions at a small-scale. For this reason, the Ru-based system is, at the current price and technological state, the most economical solution for small-scale applications, while efficient Ni-based catalysts can be the ideal choice for large scale applications.

List of symbols

c_i^b = bulk concentration of the species i (mol/L)

c_i^s = surface concentration of the species i (mol/L)

d_i = inner diameter of the reactor tube (m)

$h_f a_v$ = local heat transfer coefficient (W/(m^{2}K))

$k_g a_v$ = material transfer coefficient (mol/m^2)

k = kinetic constant (mol / ($s * gcat * ata^{5n}$))

m_i = mass of the component i (kg)

n = reaction order

n_i = number of moles of the component i (mol)

r_A = reaction rate (mol/m^{3}s)

u = speed of the gases (m/s)

x_i = molar fraction of the species i

A_0= pre-exponential factor for the adsorption rate

D = diffusion coefficient (m^2/s)

E_A = activation energy (kJ/mol)

FR_i^j = formation rate of the species j on the catalyst i (mol/m^{3}s)

K_{eq} = equilibrium constant

K_i = adsorption coefficient of the component i (kJ/mol)

LHHW = Langmuir-Hinshelwood-Hougen-Watson type model

Nu = Nusselt number

P_i = partial pressure of the component i (Pa)

Re = Reynolds number

S_p = surface of the particle (m^2)

Sh = Sherwood number

T = temeperature (K)

T_W = wall temeperature (K)

V_p = volume of the particle (m^3)

Y_i = yield to the species i

α = heat transfer coefficient (W/(m^{2}K))

χ_i = conversion of the species i

λ = heat conductivity of the gas (W/m/K)

ρ_f = density of the fluid (kg/m^3)

η = effectiveness factor of the catalyst pellet

ϕ = Thiele modulus

τ_i = residence time on the catalyst i (s)

ν_i = stoichiometric coefficient of the component i

ΔG^R = reaction free Gibbs energy (kJ/mol)

ΔH^R = reaction enthalpy (kJ/mol)

ΔH_{ADS} = heat of adsoption (kJ/mol)

Keywords: Sabatier reaction, reactor design, energy storage, economic evaluation

1. Introduction

Over the last few years, the need for efficient energy storage has boosted research into solutions that are capable of storing excess electric energy, mainly from renewable energy, in a reliable way and for long periods. In fact, with the increase in renewable energy production, a mismatch between the effective power production and the instantaneous demand is generated several times along the year. This problem could be mitigated through appropriate energy storage systems that accumulate excess energy during periods of abundance (demand below the production capacity) and re-insert it into the grid when scarcity periods (demand above the production capacity) are encountered. In this sense, chemical storage is a promising strategy to address this topic, using the so-called chemical energy carriers. Synthetic natural gas (SNG) is one of the most promising energy carriers, since it is produced from renewable hydrogen and carbon dioxide in the Sabatier reaction and is stored and distributed in already existing facilities [1,2]. The SNG produced is considered carbon neutral since the CO_2 produced in the combustion process is the same as that was used to synthesise the fuel itself [3]. Furthermore, CO_2 could be extracted from the atmosphere, while H_2 could be produced by water splitting using excess renewable energy, making the exploitation of the reaction possible even in remote locations. In this way, the renewable energy could be

produced in remote areas, and it could be transferred for consumption in the form of synthetic natural gas [4,5].

The Sabatier reaction is named after the French chemist Paul Sabatier, who first discovered the reaction of CO_2 and H_2 to give methane [6]:

$$CO_2 + 4H_2 \leftrightarrow CH_4 + 2H_2O \qquad \Delta H_0^R = -165\,\frac{kJ}{mol}$$

The Sabatier reaction is exothermic and limited by thermodynamic equilibrium. In stoichiometric conditions, 99% CO_2 conversion is only achieved at temperatures below 300°C [7]. Equilibrium CO_2 conversion is increased with increasing pressure, following the decrease in the number of moles in the course of the reaction. For this reason, an appropriate catalyst is required to perform the reaction with high methane yield. Several catalysts have been proposed for the Sabatier (and CO methanation) reaction. Metals of the VIII B group are reported as good catalysts for the reaction [8]; among them, Ni is the most commonly used on an industrial scale. Several studies have reported various supported Ni catalysts for the Sabatier reaction; typical supports are Al_2O_3, SiO_2, TiO_2, CeO_2, or ZrO_2. Catalysts with high nickel load supported on aluminium or titanium oxide are known to be already active at temperatures below 300°C [9–11]. However, Ni-based catalysts are subjected to various undesired phenomena, such as carbide [12] and polycarbonyl [13] formation, resulting in deactivation by sintering [5] and volatilisation [14].

Ru-based catalysts are a valid alternative to Ni. Ru is particularly active in the Sabatier reaction [8], and is supported by various oxides, such as Al_2O_3 [15,16], TiO_2 [17,18], and CeO_2 [19,20]. Ru/Al_2O_3 is reported to be already active at 200°C which makes it possible to reach a CO_2 conversion of above 99% with an appropriate reactor design [21]. Furthermore, Ru-based catalysts are less prone to deactivation than the other methanation catalysts [22]. Some deactivation phenomena due to carbon fouling have been reported in the literature when gas feeds containing CO are used [23]. However, this higher performance in the Sabatier reaction is counterbalanced by the high cost of the material.

In order to address the dispute between Ru- and Ni-based catalysts for the development of Sabatier reactors for the production of SNG, this paper offers a simulation study to compare the performance of the two catalysts in terms of productivity and relative catalyst load. In section 3.1, we analyse the parametric sensitivity of the Sabatier reactor over Ni-based

catalysts and compare it to the Ru/Al_2O_3 case. We underline how the reactor activation is a crucial parameter in determining the performance of the entire reactor and the possibility of heat integration of an SNG production process. In section 3.2, we compare the calculated reaction rate of the catalysts and underline how the diffusion limitation differently affects the two systems. With the reaction rate being much higher over Ru/Al_2O_3, the latter is more prone to developing intraphase limitations, with important consequences at the hotspot location inside the reactor. In section 3.3 we show that, due to heat transfer limitations, the $Ni/Mg/Al_2O_4$ catalyst shows the same performance as Ru/Al_2O_3 in a key part of the reactor, indicating that a high-performing catalyst is not required in this section. For this reason, section 3.4 is dedicated to a design study of a Ru/Ni hybrid reactor. Finally, in section 3.5, we analyse the amount of catalyst required to reach various levels of CO_2 conversion. Since the analysed $Ni/Mg/Al_2O_4$ cannot reach a conversion higher than 95% due to the high activation temperature, we introduced an Ni/Al_2O_3 catalyst to the comparison. This catalyst showed a lower activation temperature, and thus was able to reach, with intermediate condensation steps, the same performance as the Ru/Al_2O_3 catalysts. On the basis of the simulation results, we performed an economic analysis to determine the difference in cost for the installation of the two reactive systems analysed. In this framework, the production of an SNG that can be directly injected into the natural gas grid was set as the target.

2. Materials and methods

2.1. Kinetics

To determine the performance of Sabatier reactors operating with Ru/Al_2O_3, $Ni/Mg/Al_2O_4$, and Ni/Al_2O_3, the kinetic models of Falbo et al. [24], Xu and Froment [25], and Koschany et al. [10] were used. The first model was in the form of a power law. The models for the Ni-based catalysts were developed according to the Langmuir–Hinshelwood mechanism. Unfortunately, no model reflecting the L–H mechanism for industrially relevant conditions over Ru/Al_2O_3 is currently available in the literature [24]. Furthermore, no explicit kinetic law exists for the water-gas-shift (WGS) reaction on the same catalyst. However, WGS reaction is fast over this catalyst, so that it is possible to model the latter reaction as an equilibrium reaction. This is confirmed by several experimental reports [24,26–28]. The parameters of the kinetic models are reported in Tables 1 (Ru/Al_2O_3), 2 ($Ni/Mg/Al_2O_4$), and 3 (Ni/Al_2O_3).

The CO_2 conversion is defined as:

$$\chi_{CO2} = \frac{n_{CO2,IN} - n_{CO2,OUT}}{n_{CO2,IN}} \quad (1)$$

The CO yield is defined as:

$$Y_{CH4} = \frac{n_{CO,OUT}}{n_{CO2,IN}} \quad (2)$$

The methane yield is defined as:

$$Y_{CH4} = \frac{n_{CH4,OUT}}{n_{CO2,IN}} \quad (3)$$

Table 1. The parameters of the kinetic model from Falbo et al. [24] *(Ru/ Al_2O_3).*

Equation rate	Reaction order (n)	k_0 $[mol/(s \cdot gcat \cdot ata^{5n})]$	E_A [kJ/mol]
$r_{CO2} = k\left\{[P_{CO2}]^n[P_{H2}]^{4n} - \frac{[P_{CH4}]^n[P_{H2O}]^{2n}}{K_{eq}(T)^n}\right\}$	0.076	18.26	65.2

Table 2. The parameters of the kinetic model from Xu and Froment [25] *(Ni/Mg/Al_2O_4).*

Equation rate	$\boldsymbol{k_0}$	$\boldsymbol{E_A}$ [kJ/mol]
$\boldsymbol{r_{SR}} = \frac{\frac{k_{SR}}{P_{H_2}^{2.5}}\left(P_{CH_4}P_{H_2O} - \frac{P_{H_2}^{3}P_{CO}}{K_{eq,SR}}\right)}{DEN^2}$	4.225×10^{15}	240.1
$\boldsymbol{r_{WGS}} = \frac{\frac{k_{WGS}}{P_{H_2}}\left(P_{CO}P_{H_2O} - \frac{P_{H_2}P_{CO_2}}{K_{eq,WGS}}\right)}{DEN^2}$	1.995×10^{6}	67.13
$\boldsymbol{r_{SAB}} = \frac{\frac{k_{SAB}}{P_{H_2}^{3.5}}\left(P_{CH_4}P_{H_2O}^2 - \frac{P_{H_2}^{4}P_{CO_2}}{K_{eq,SAB}}\right)}{DEN^2}$	1.020×10^{15}	243.9
$\boldsymbol{DEN = 1 + K_{CO}P_{CO} + K_{H_2}P_{H_2} + K_{CH_4}P_{CH_4} + \frac{K_{H_2O}P_{H_2O}}{P_{H_2}}}$		

Parameter	A_0	ΔH_{ADS} [kJ/mol]
$\boldsymbol{K_{CO}}$	8.23×10^{-5}	-70.65
$\boldsymbol{K_{H_2}}$	6.12×10^{-9}	-82.90
$\boldsymbol{K_{CH_4}}$	6.65×10^{-4}	-38.28
$\boldsymbol{K_{H_2O}}$	1.77×10^{5}	88.68

Table 3. The parameters of the kinetic model from Koschany et al. [10] *(Ni/Al_2O_3).*

Equation rate	$\boldsymbol{k_0}$	$\boldsymbol{E_A / \Delta H_{ADS}}$ [kJ/mol]
$\boldsymbol{r_{Sab}} = \frac{kP_{H_2O}^{0.5} P_{CO_2}^{0.5} \left\{1 - \frac{P_{CH_4} P_{H_2O}^2}{P_{CO_2} P_{H_2}^4 K_{eq}}\right\}}{\left(1 + \frac{K_{OH} P_{H_2O}}{P_{H_2}^{0.5}} + K_{H_2} P_{H_2}^{0.5} + K_{mix} P_{CO_2}^{0.5}\right)^2}$		
$\boldsymbol{k}$	3.46×10^{-5}	77.5
$\boldsymbol{K_{OH}}$	0.50	22.4
$\boldsymbol{K_{H_2}}$	0.44	-6.2
$\boldsymbol{K_{mix}}$	0.88	-10.0

2.2. Model of the fixed bed reactor

The reactor was modelled with a one-dimensional heterogeneous plug flow reactor (PFR) model. The reactor was modelled with canonical mass and energy balances [29]. For the computation of the intraphase mass transfer limitations, the effectiveness factor model was used [29,30]. The model equations for the fluid phase are:

$$\frac{\partial (u c_i)}{\partial z} = k_g a_v (c_i^b - c_i^s) \tag{4}$$

$$\left(u \rho_f c_{tot} c_p\right) \frac{\partial T}{\partial z} = h_f a_v (T^s - T) - \frac{4}{d_i} \alpha \left(T - T_{cf}\right) \tag{5}$$

The balance equations for the solid are:

$$k_g a_v\left(c_i^b - c_i^s\right) = \upsilon_{i,wgs}\eta_{wgs}\rho_b r_{wgs} + \upsilon_{i,sab}\eta_{sab}\rho_b r_{sab} + \upsilon_{i,sr}\eta_{sr}\rho_b r_{sr} \quad (6)$$

$$k_f a_v(T^s - T) = \eta_{wgs}\rho_b(-\Delta H_{wgs})r_{wgs} + \eta_{sab}\rho_b(-\Delta H_{sab})r_{sab} + \eta_{sr}\rho_b(-\Delta H_{sab})r_{sr} \quad (7)$$

Additionally, the heat balance of the cooling fluid is solved to determine the cooling temperature:

$$-\left(u\rho_{cf}c_p\right)\frac{\partial T}{\partial z} = \frac{4}{d_i}\alpha\left(T - T_{cf}\right) \quad (8)$$

The cooling is counter-current and performed with molten salts.

The thermodynamic equilibrium constant for the Sabatier reaction is calculated as [24]:

$$K_{eq}(T) = \exp\left(\left(\frac{1}{1.187}\right) \times \left(\frac{56000}{T^2} + \frac{34663}{T} - 16.4\,ln(T) + 0.00557 \times T\right) + 33.165\right)$$

(9)

The thermodynamic equilibrium constant for the water gas shift reaction is calculated as [31]:

$$K_{eq}(T) = 9.01 \times 10^{-6}(T)^{0.968}\exp\left(\frac{\Delta G}{RT}\right) \quad (10)$$

Where $\Delta G = 43.6\ kJ/mol$.

The superficial velocity of the gas phase was calculated by the continuity equation (Equation 11):

$$u_s(z) = u_{s,0}\frac{\rho_0}{\rho(z)} \quad (11)$$

The effectiveness factor (degree of utilisation of the catalyst) was calculated for each reaction with the formula of the spherical pellet:

$$\eta_r = \frac{3}{\phi^2}(\phi\coth(\phi) - 1) \quad (12)$$

The Thiele modulus was used in its generalised form as follows (the kinetic order was calculated from linearisation of $n = p_i\frac{\partial \ln(r)}{\partial(P_i)}$ for the kinetic models of Ni-based catalysts):

$$\phi = \frac{V_p}{S_p}\sqrt{\frac{n+1}{2}\frac{kC_{i,s}^{n-1}}{D}} \quad (13)$$

The boundary conditions are:

$$c_i = c_i^0 \tag{14}$$

$$T = T^0 \tag{15}$$

$$T_{cf} = T_{cf}^0 \tag{16}$$

The CO_2 and H_2 were fed in stoichiometric amounts (1:4) and without dilution. The dimensions of the reactor were kept constant in the various cases studied. The pressure drop along the axial coordinate of the reactor was neglected. The heat losses towards the external environment were neglected (the reactor was considered as fully insulated). α is the global effective heat transfer coefficient, and was calculated using the analogy with a series of thermal resistances. The resistances considered were the effective heat transfer coefficient inside the tube, outside the tube, and the conductivity of the tube wall. The resulting formula is:

$$\frac{1}{\alpha} = \frac{1}{k_i} + \frac{k_c}{ln\left(\frac{r_i}{r_e}\right)} + \frac{1}{k_e} \tag{17}$$

k_e is set constant to 2000 W/(m^{2}K) and k_i is calculated with an appropriate correlation for the Nusselt number [32]:

$$Nu = \frac{k_i d_p}{\lambda_g} \tag{18}$$

The thermal properties of the gases are approximated by polynomials according to VDI–Wärmeatlas [33]. The heat and mass transfer coefficients for the particle-to-fluid transfer are approximated by Wakao's correlation [34]:

$$Sh = 2 + 1.1\, Sc^{\frac{1}{3}}\, Re^{0.6} \tag{19}$$

$$Nu = 2 + 1.1\, Pr^{\frac{1}{3}}\, Re^{0.6} \tag{20}$$

2.3. Computational methods

The system of differential equations (Equations 4, 5, and 8) was reduced to two mass balances and two heat balances by substitution of the concentration of the various components (CO_2, H_2, CH_4, H_2O, CO) with the CO (Equation 2) and CH_4 yield (Equation 3).

The resulting equations constitute a differential-algebraic equations (DAE) system, together with the Equations (6) and (7). The DAE system was integrated numerically over the axial reactor coordinate using the MATLAB ode23t solver.

3. Results

3.1. Parametric sensitivity

The Sabatier reaction is a strongly exothermic reaction and it is characterised by parametric sensitivity, which means that, in the reactor, a small change in a single parameter can generate an important modification in the reactor performance. In the CO_2 methanation reactor, the parametric sensitivity is present in the light-off of the reactor: the feed temperature, together with other parameters, such as pressure and space velocity, determine the possibility of correctly operating the reactor. If these conditions are not reached, the reactor will work at low temperatures, meaning that low CO_2 conversion values are obtained. In our previous study [35], we analysed the parametric sensitivity of the Sabatier reaction over Ru/Al_2O_3 in detail. Here, we briefly summarise the results and compare the activation requirements of the Ru-based system with an equivalent commercial $Ni/Mg/Al_2O_4$ catalyst. This latter catalyst was selected to underline the maximal difference that can exist in parametric sensitivity between the Ru/Al_2O_3 catalyst and a Ni-catalyst with a low performance in the CO_2 methanation reaction. In this way, the extreme limits for the operation with a Ni-based catalyst are set; any specifically new-synthesized Ni-based catalyst should improve these results. The first comparison concerns the activation of a single-stage adiabatic reactor. The analysis of this system is relatively easy because of the absence of cooling. In this case, the most important parameters for reactor activation are the inlet temperature and pressure, as well as the space velocity. The activation temperature with Ru and Ni as a function of pressure at a space velocity of 3000 h^{-1} is shown in Figure 1. Activation temperature is the minimal feed temperature required to assure the normal operation of the reactor and to avoid the reactor deactivation due to lack of thermal self-sustain of the reaction. The difference in activation temperature is large within the entire pressure interval considered, ranging from 100°C at low pressure to ca. 80°C at high pressure. Note that the decrease in activation temperature with pressure is different for the two catalysts considered due to the different nature of the kinetic models used (the power law for Ru/Al_2O_3 and the LHHW for $Ni/Mg/Al_2O_4$). The difference in the two models is made evident by the speed at

which an asymptotic value of $Ni/Mg/Al_2O_4$ was reached due to the surface saturation at high pressure. However, no kinetic model for Ru/Al_2O_3 following the LHHW scheme for a large range of parameters is available in the literature [36].

$Ni/Mg/Al_2O_4$ is the reference system for the commercial Ni catalysts. However, the recent effort for the development of a transition metal catalyst specific for the CO_2 methanation reaction lead to the synthesis of improved materials for this scope. Here, we introduce in the comparison a high-performing Ni/Al_2O_3 catalyst specifically developed for the Sabatier reaction [10]. Figure 1 is complemented by the information regarding this specific catalyst (solid line with squares). The difference in light-off temperature between Ru/Al_2O_3 and Ni/Al_2O_3 is much smaller than in the case previously discussed, and it is about 20 °C in favour of Ru. This means that a substantially similar activation curve can be drawn using Ru and a high-performing Ni-based catalyst.

The comparison of the activation temperature required for the two systems in a cooled reactor is more complex, since the performance is influenced by the properties of the cooling system. Figure 2 shows the change in the difference in activation temperature for a standard cooled reactor operated with $Ni/Mg/Al_2O_4$ or Ru as a function of temperature (solid line). The cooling parameters, selected to be representative of a reactor characterised by a moderate level of heat exchange, are: a cooling temperature of 180°C (according to thermodynamic limitations for the system considered [35]), and a diameter of the pipe of 0.02 m. The difference in activation temperature is important for low pressure since the commercial Ni catalyst considered is not very active under these conditions. At 1 bar, the difference is ca. 100°C. A pressure increase favours the activity of the catalyst so that the activation temperature difference decreases to a minimum at 4 bar. Above this value, the temperature difference increases again due to the saturation phenomenon that has already been mentioned. In any case, the difference in activation temperature remains above 55°C in the entire parametric range considered. This has an important consequence in the reactor design because the feed stream is preheated to higher temperatures in the case of Ni, making the heat integration of the system more challenging. This phenomenon constitutes the main difference between the two catalytic systems investigated and the practical effects on reactor design will be analysed in detail in the following sections. The light-off temperature in a cooled reactor can be reduced by using the state-of-the-art Ni/Al_2O_3 catalyst, as shown in figure 2

(dotted line). In this case, a difference in the activation temperature compared to Ru is still present, but it is limited to ca. 20-30 °C in the entire pressure range investigated. This means that the Sabatier reactor operating with this catalyst can be activated similarly to the Ru case, but a special focus should be devoted to the heat integration, as the gases must be pre-heated at a level above the reactor outlet temperature (ca. 200-220 °C).

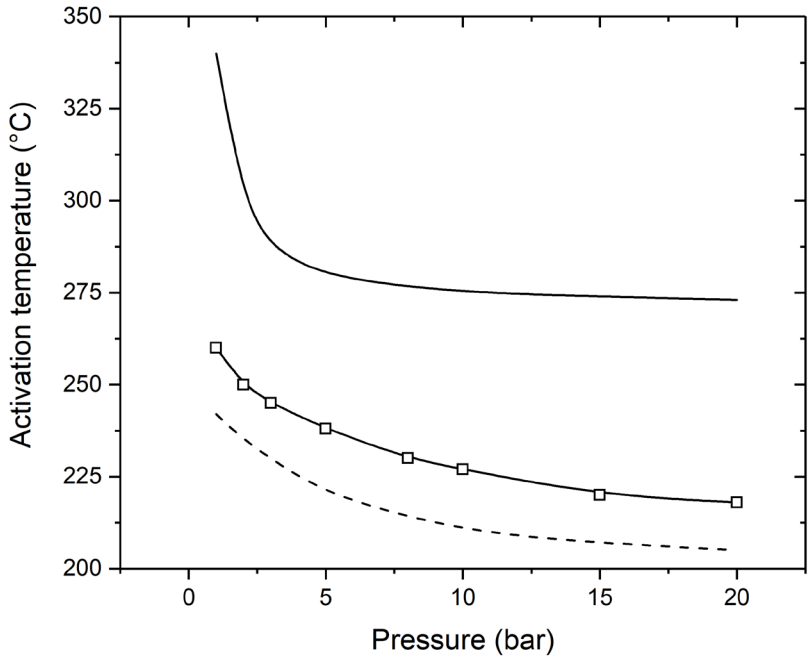

Figure 1. Variation of the activation temperature with pressure in an adiabatic reactor operating with – Ni/Mg/Al_2O_4, -□ Ni/Al_2O_3 and - - Ru (GHSV = 3000 h^{-1})

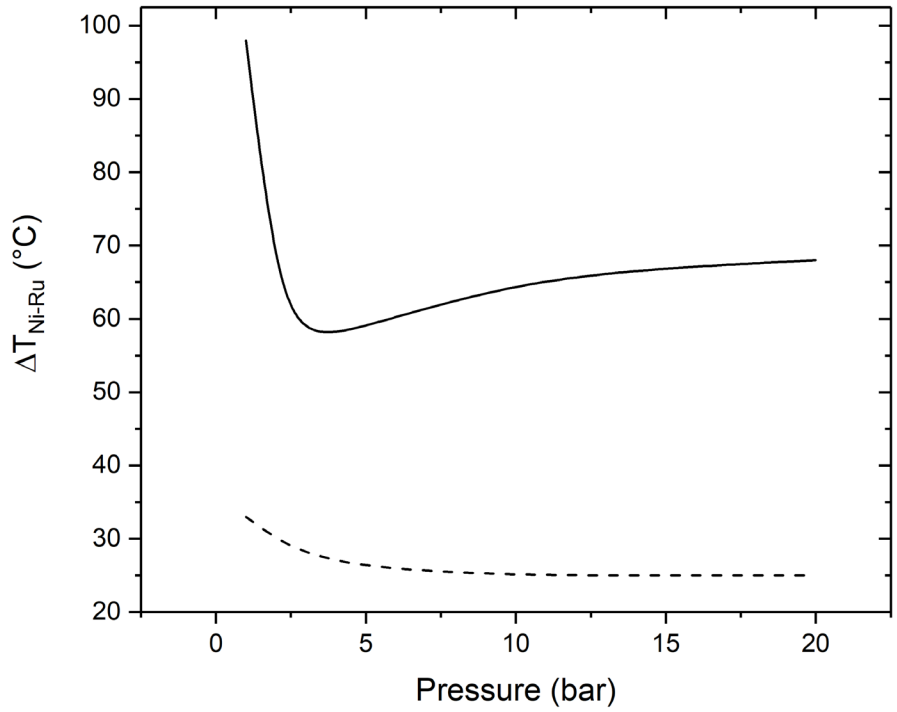

Figure 2. The difference in activation temperature between Ni/Mg/Al_2O_4 and Ru (- solid line) and between Ni/Al_2O_3 and Ru (-- dashed line) with pressure in an externally cooled reactor (GHSV = 3000 h^{-1}, T_c = 180°C, D_i = 0.02 m)

3.2. Implications of differences in reaction rate

The reaction rate is calculated according to the two considered kinetic models, fixing the temperature and the partial pressure of the various species. The partial pressures are calculated from the methane yield as follows:

$$P_i = P \times x_i = P \times (x_i^0 + \frac{n^0 \times (\sum_{j=1}^{NR} v_{i,j} \times Y_j)}{\sum_{k=1}^{NS} n_k}) \quad (21)$$

Where P_i is the partial pressure of the component i, P the total pressure, x_i^0 the molar fraction of the component i, v_i the stoichiometric coefficient of the component i, and Y the CH_4 yield.

In this way, it is possible to plot the methane formation rate values in a temperature vs. CH_4 yield graph. Formation rate refers to the sum of all the reaction rates that lead to the formation of methane. The most suitable indicator to compare the reaction rates over the two catalysts considered is the formation rate ratio:

$$Rate\ ratio_{Ni/Ru} = \frac{FR_{Ni}^{CH_4}(T,\eta)}{FR_{Ru}^{CH_4}(T,\eta)} \quad (22)$$

The values of this indicator as a function of temperature and yield are shown in Figure 3a. At low temperatures (T < 400°C), the reaction rate of Ru is much higher than that of Ni for every yield value, so that the ratio assumes values lower than 0.01. In the temperature range 400°C < T < 600°C, the indicator is strongly dependent on the yield, with a minimal difference close to the thermodynamic equilibrium line. The decrease in the indicator is due to two different phenomena according to the yield value. At low yield and high temperature, the activity of the Ni catalyst in the Sabatier is higher, reaching values up to 0.05 times the rate of Ru under the same conditions. At high yield, the forward reaction rate is low, approaching thermodynamic equilibrium. Since the equilibrium is independent of the catalyst used, the reaction rate tends to be the same for both catalysts. This specific aspect of the Sabatier reaction is of particular importance for the reactor design and is further analysed and discussed in the following sections. At high temperatures (T > 600°C), the rate ratio decreases again, due to the already mentioned difference in the kinetic models used (power law vs. LHHW). The discussion of the performance of the two catalysts in this region is, however, of low importance for the reactor design, since the yield is limited by thermodynamics.

The previous discussion focused on the determination of the intrinsic kinetics for the two catalytic systems considered. However, the Sabatier reaction is characterised by high absolute values of intrinsic kinetics, so that the reaction is affected by significant diffusion limitations. In order to evaluate these phenomena, the results of Figure 3a were recalculated considering the effective reaction rate, as per the generalised Thiele modulus. For both catalysts, a standard commercial cylindrical pellet with a 1 mm characteristic dimension is considered. Due to the high reaction rate, the Ru/Al_2O_3 catalyst is subject to more severe diffusion limitations than the $Ni/Mg/Al_2O_4$ system. The degree of utilisation of the catalyst at the inlet conditions for Ru starts decreasing from 1 below 300°C. However, the diffusional limitations of Ni appear only above 500°C. The minimal temperature for appearance of diffusional limitations over the two catalysts is reported in table 4. As a consequence, the picture from Figure 3a is partially modified when considering the effect of the degree of utilisation of the catalyst. Figure 3b shows the new map of the $Rate\ ratio_{Ni/Ru}$.

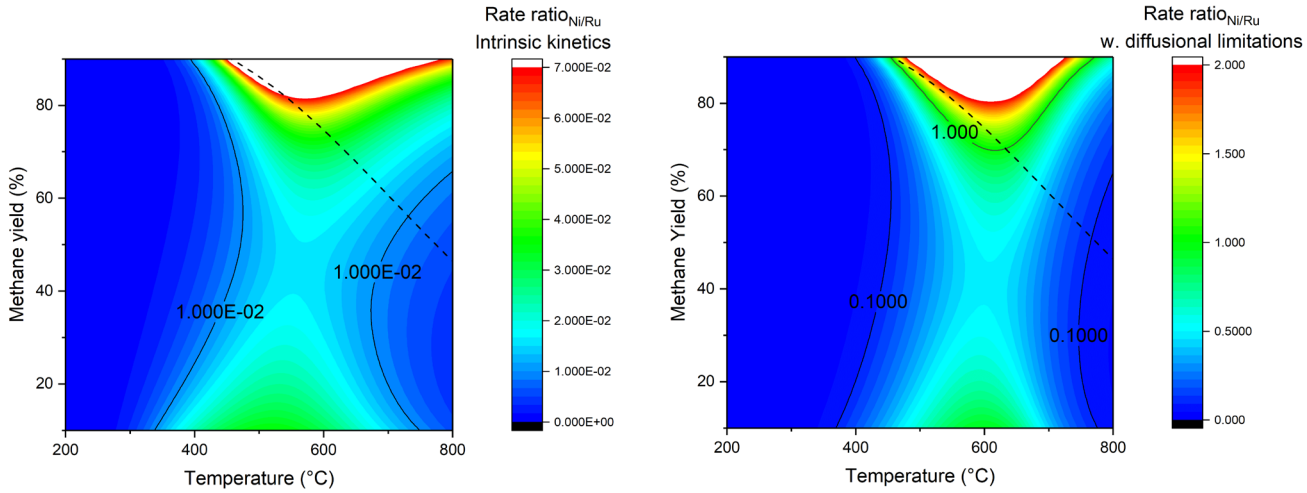

Figure 3. The methane formation rate ratio of the Sabatier reaction for Ni and Ru: a) intrinsic kinetics, b) effect of diffusion limitations included (-- thermodynamic equilibrium)

Table 4 Minimal temperature for appearance of diffusional limitations over Ni/Mg/Al_2O_4 and Ru/Al_2O_3

Catalyst	Ru/Al_2O_3	Ni/Al_2O_3	Ni/Mg/Al_2O_4
T for $\phi = 0.9$	250 °C	300 °C	600 °C

At temperatures below 300°C, no significant differences are found, and the problem concerning the high-temperature required for activation of the Ni catalyst remains. In the intermediate temperature range, the results are modified compared to Figure 3a, and the relative difference in reaction rate is reduced by about one order of magnitude. In particular, in the area close to the thermodynamic equilibrium at high conversion, the reaction rates are practically identical. This means that the catalyst is completely controlled by diffusion, which limits the reaction rate, cancelling the intrinsic difference between the two catalysts. This is an important result to consider when performing the reactor design, which is the subject of the following section.

If we extend the comparison to the Ni/Al_2O_3, we can observe how the methane formation rate chart becomes more similar to Ru/Al_2O_3. The formation rate ratio for these two catalysts is shown in figure 4. The formation rate over Ni/Al_2O_3 is 10 times lower below 300 °C (black line on the left of the graph), but it increases quickly above this temperature, reaching the

equivalence line (Rate ratio = 1) between 500-600 °C at most of the yield values investigated. Hence, we can conclude that this state-of-the-art Ni catalyst shows the same performance as the Ru catalyst above 300 °C, while the Ru/Al_2O_3 is more active below this threshold. For this reason, the use of a hybrid bed (Ni+Ru) can be beneficial also with the Ni/Al_2O_3 catalyst.

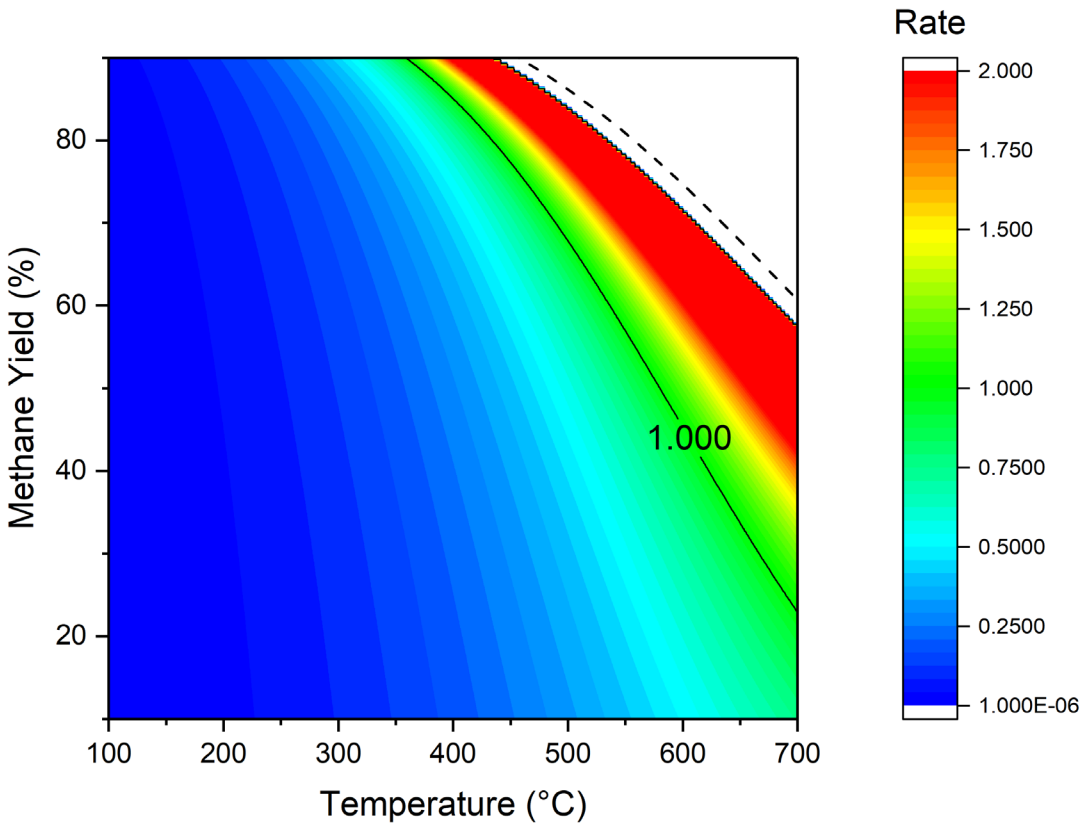

Figure 4. The methane formation rate ratio for the Sabatier reaction over Ni/Al_2O_3 and Ru/Al_2O_3

3.3. Design of a fixed bed Sabatier reactor

On the basis of the previous results, we performed a reactor design routine to analyse the differences in the performance of two Sabatier reactors operating with Ru/Al_2O_3 and $Ni/Mg/Al_2O_4$, respectively. The main parameters of the two reactors are reported in Table 5. We compared the performance of the two reactors in the temperature vs. the methane yield space; the results are shown in Figure 5. $Ni/Mg/Al_2O_4$ was chosen as reference catalyst for this study in order to underline the part of the reactor where even a Ni catalyst with poor performance can substitute Ru/Al_2O_3. This study wants to set the framework of the maximum

difference that can exist between a Ru and a Ni catalyst. As mentioned in section 3.1, the reaction activates at a different temperature for Ru and Ni, with the light-off temperature for Ni being ca. 100°C higher than that for Ru. The temperature initially rises in a practically adiabatic way over Ru/Al_2O_3, until reaching the thermodynamic limit. In this case, the yield to methane in this part of the reactor is ca. 50%, and the temperature rise is greater than 400°C. The initial part of the Ni reactor operates in a substantially different way. The delayed activation temperature reduces the extent of the hotspot due to the smaller distance to the thermodynamic limit. Furthermore, the lower reaction rate allows better control of the reaction, so that part of the reaction heat is removed before reaching thermodynamic equilibrium. For these reasons, the extent of the hotspot is ca. 50° lower than the Ru case. When the thermodynamic equilibrium is reached, the reaction is controlled by cooling. The removal of heat is the governing parameter, meaning that the reaction rate is the same for both catalysts. In this part of the reactor, the optimisation must involve the adaptation to the heat transfer properties only. We named this section of the reactor the 'equivalence area' as all catalysts showed the same performance. The use of an improved Ni-based catalyst, such as Ni/Al_2O_3, increases the extension of this area.

Table 5 Parameters of the reactor used for comparison

Parameter	**Value**
Pressure (bar)	10
Inner tube diameter (m)	0.02
Catalyst density (kg/m^3)	1500
CO_2: H_2 ratio (-)	1:4
Pellet diameter (mm)	1
Catalyst void ratio (-)	0.6

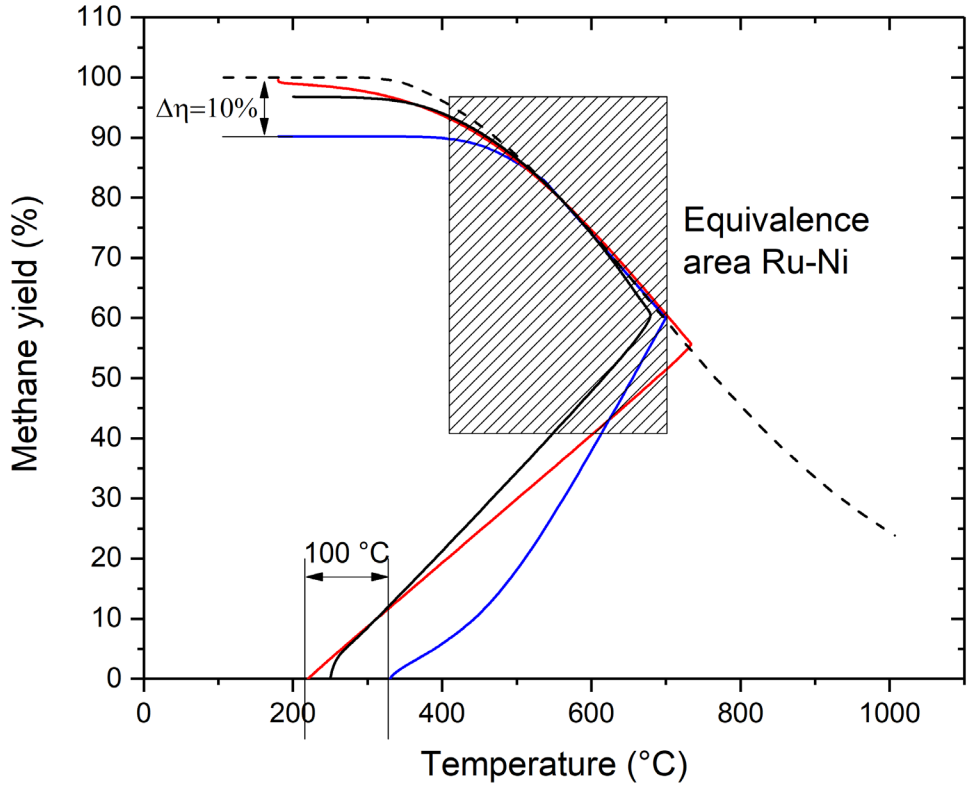

Figure 5. The trajectory of the temperature vs. methane yield (- Ni/Mg/Al_2O_4, -Ni/Al_2O_3 - Ru, - - equilibrium)

The 'equivalence area' is extended until a point in the temperature-conversion space where the cooling rate becomes higher than the heat production rate by the chemical reaction. In Figure 5, this point is found at 450°C and 85% yield of methane. Below this threshold, the activity of the Ni/Mg/Al_2O_4 is too low to compensate for the reactor cooling, so the outlet yield is limited to less than 90%. Ru/Al_2O_3 is still active at this temperature and the reactor operating with this catalyst can reach yields of close to 100%. From these results, we can observe that the key to the high-performing Sabatier reactor is the low-temperature activity. The light-off temperature is a significant parameter determining the extent of the hotspot, the conversion before reaching equilibrium, and the residence time required to reach the hotspot. However, the poor performance of a catalyst in this phase could be compensated by an appropriate reactor design and good heat integration. The last part of the reactor is the most important section of the reactor, and determines the global performance of the reactive system. Ni/Mg/Al_2O_4 could not provide full CO_2 conversion in a single pass reactor so a special reactor design is necessary to overcome the limitations. The considerations here presented remain substantially unchanged using the Ni/Al_2O_3 catalyst, with the difference that the

equivalence area would be extended and that the light off temperature is similar for the two catalysts, so that Ni/Al_2O_3 can be used already in the reaction activation region. In the next sections, we will analyse the design and assessment of some strategies to overcome these limitations.

3.4. Design of a hybrid-bed Sabatier reactor

As observed in the previous section, the performance of the Ni/Mg/Al_2O_4 catalyst is substantially similar to the Ru/Al_2O_3 up to a CO_2 conversion of approximately 85%. Based on this observation, it appears interesting to design a hybrid reactor, comprised initially of a Ni bed followed by a Ru-based part to complete the CO_2 conversion. We simulated a fixed-bed Sabatier reactor following this concept using the quantity of Ru/Al_2O_3 to be introduced into the reactor as an optimisation parameter. The optimisation function is:

$$\min_{m_{Ru}} \tau_{reactor} = f(m_{Ru})$$

$$s.t. Y_{CH4} > 0.995$$

Where τ_{Ru} is the residence time in the reactor over the Ru catalyst.

In this problem, we only optimised the quantity of Ru, without any limitations of the quantity of Ni or the total reactor volume. This means, on the one hand, that the reactor section operating with Ni is not optimised and, on the other hand, that the total volume of the reactor is not designed to the absolute optimum.

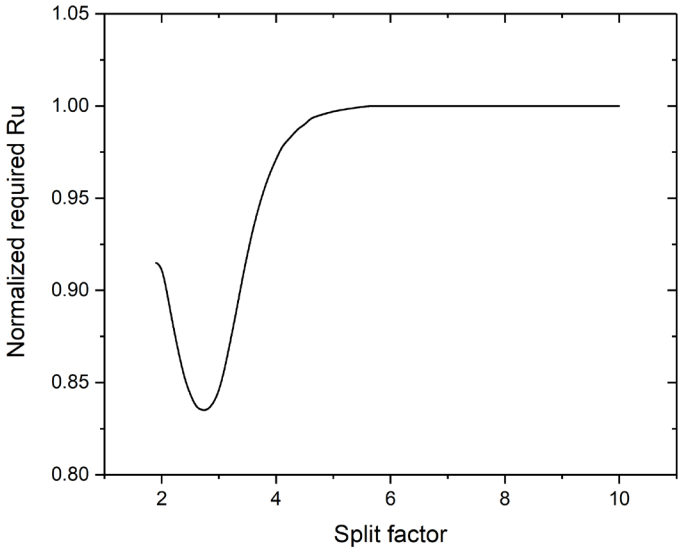

Figure 6. The normalised amount of Ru/Al_2O_3 required in the hybrid-bed to reach 99.5% yield of methane as a function of the amount of $Ni/Mg/Al_2O_4$

The results of the optimisation procedure are shown in Figure 6. The x-axis refers to the split factor, that is the ratio between the weight of Ni catalyst in the reactor and the total amount of catalyst. The function shows an evident minimum, the origin of which is explained by the graphs in Figure 7. The reactor is operated in every case on Ni until the conversion of 85%. Note that in this procedure we allowed reaching a hotspot temperature over the Ni bed that may be too high for this catalyst. The difference in the split points can be seen as a modification in the inlet temperature in the part of the reactor operating with the Ru bed. With a low amount of Ni (right side curve in Figure 7), the inlet temperature is high (T > 400°C), so the reaction trajectory matches the thermodynamic equilibrium line after a limited hotspot. This results in reduced performance of the Ru catalyst since the reaction is controlled by cooling for part of the catalytic bed. An enlargement of the Ni reactor section (central curve of Figure 7) provokes a decrease in the initial requirement for Ru since the cooling-controlled section of the latter catalytic bed is reduced. This decrease in the residence time of Ru continues until a minimum point, whose localisation varies depending on the cooling properties of the reactor. After the minimum, the requirement for Ru increases because the inlet temperature to the second catalytic bed is too low (below 220°C) and the reaction starts with a high reaction rate. In conclusion, the minimisation of the amount of Ru necessary to reach the 99.5% CO_2 conversion specification after the $Ni/Mg/Al_2O_4$ catalytic bed is found as a compromise to the requirement of a high reaction

rate (high temperature needed) and the need to avoid the control of cooling (low temperature required). This optimisation procedure depends strongly on the cooling properties of the system, such as the coolant temperature, properties, space velocity, and reactor geometry.

In this section, we used Ni/Mg/Al_2O_4 as a reference Ni catalyst to underline the effect of Ru as a reaction-completing catalyst. However, the same considerations can be made using a Ni catalyst more active in the CO_2 methanation, with the consequence that the required amount of Ru would be decreased, and limited to the area at methane yield above 95 %.

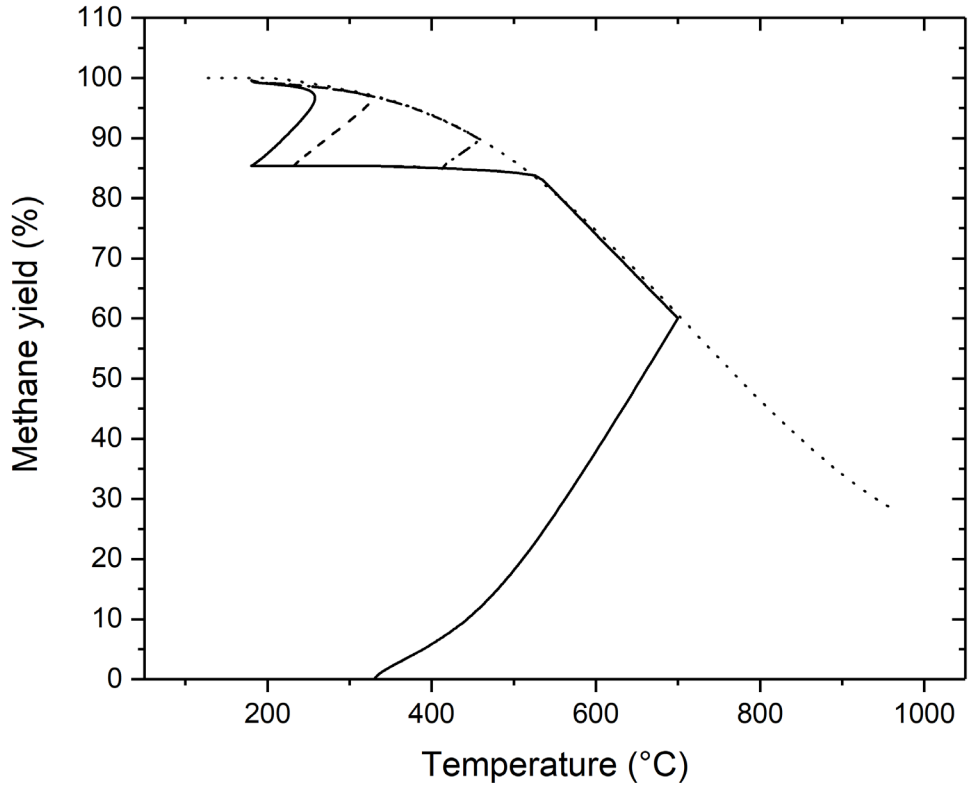

Figure 7. The trajectory of the temperature yield space of the hybrid- bed reactor for various split points: - - optimal split point; - split point causing overcooling; - · - split point causing operation in heat transfer control.

3.5. Comparison of reactors based on Ru and Ni catalysts

Based on the previous results, we propose a final comparison of the Ru and Ni-based Sabatier reactors. In order to correctly address the analysis, we compared Ni/Mg/Al_2O_4, Ni/Al_2O_3 and Ru/Al_2O_3. We divided the comparison into two parts: below and above a 95% methane yield. Figure 8 shows the normalised reactor volume to reach 70%, 90%, and 95% methane yield on Ru/Al_2O_3, Ni/Al_2O_3, and Ni/Mg/Al_2O_4, respectively. The reference point is

the residence time required to reach 99% conversion of Ru/Al_2O_3. At a low methane yield, the difference between the three catalysts is important: Ru/Al_2O_3 requires six times less catalyst volume than Ni/Al_2O_3 and nine times less than $Ni/Mg/Al_2O_4$. This difference is mainly due to the different inlet temperature, which increases the fraction of the conversion achieved in the pseudo-adiabatic section of the reactor. When increasing the methane yield achieved, the difference between catalysts decreases. The catalyst volume ratio accounts for 3.11 for Ni/Al_2O_3 and 4.42 for $Ni/Mg/Al_2O_4$ at a 90% methane yield. This latter catalyst cannot produce more than 90% yield in the single-pass reactor, so an intermediate condensation step is required to remove water and shift the thermodynamic equilibrium. Figure 9 shows the normalized required reactor volume to reach 99% and 99.5% methane yield on Ru/Al_2O_3, Ni/Al_2O_3 and on a hybrid reactor. We can observe that the Ni/Al_2O_3 reactor requires an intermediate condensation step in both cases. With this technical solution, the catalyst volume required is 2 times higher compared to Ru/Al_2O_3 for 99% yield and 1.89 for 99.5% yield. This reduction in the volume ratio is due to the different thermodynamic limit existing for the two systems, originating from the condensation step. The hybrid bed reactor shows an intermediate performance, with a volume ratio to Ru/Al_2O_3 of 1.38 for both 99% and 99.5% yield. Advantage of the hybrid bed compared to a single Ni-based catalytic bed is the absence of the intermediate condensation step, while the advantage to the Ru/Al_2O_3 system is the lower cost, due to the substitution of part of the Ru with Ni. These characteristics make the hybrid bed reactor an interesting candidate for the implementation of the Sabatier reactor in energy storage systems.

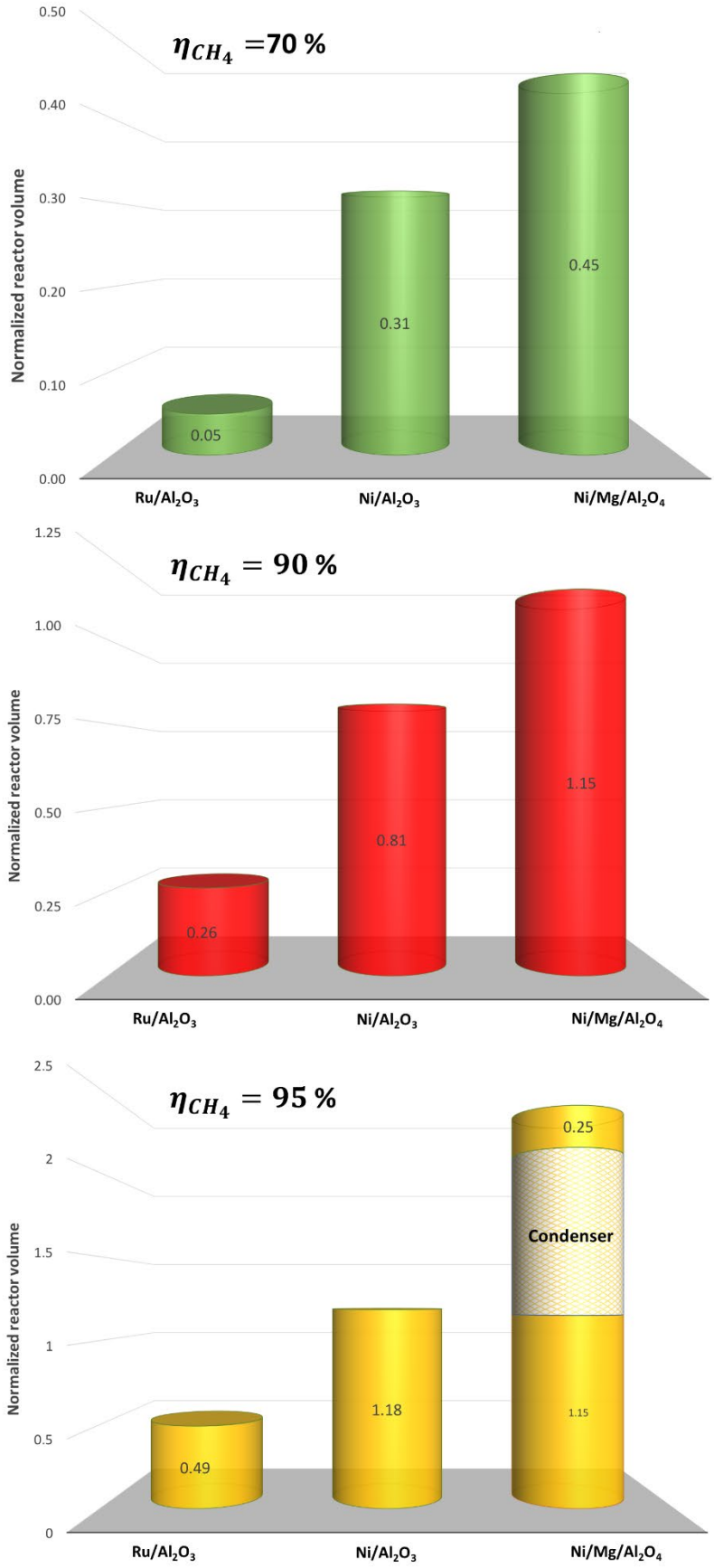

Figure 8 Required residence time to reach 70 %, 90 % and 95 % methane yield on Ru/Al_2O_3, Ni/Al_2O_3 and $Ni/Mg/Al_2O_4$ respectively

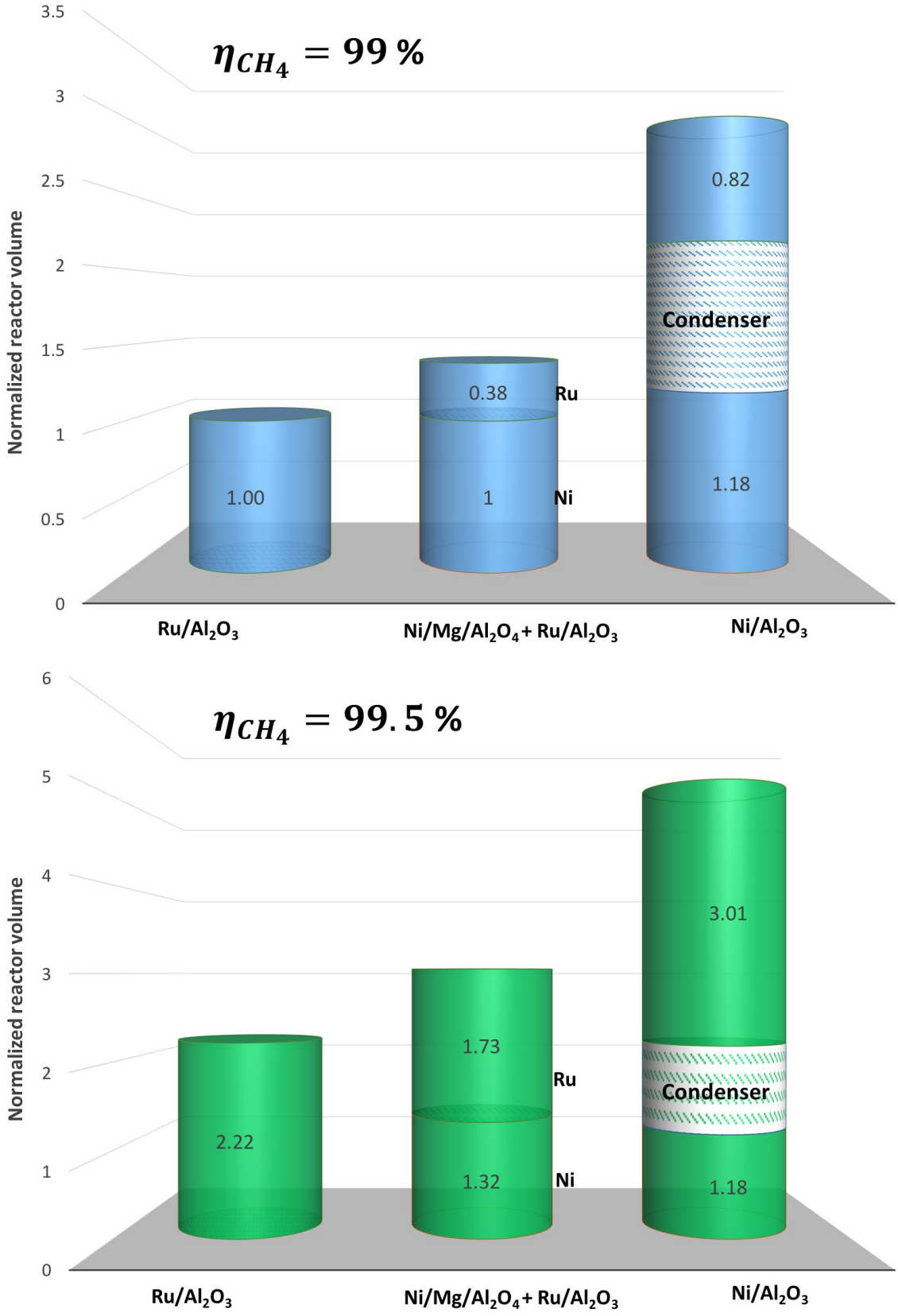

Figure 9. The required residence time to reach 99% and 99.5% methane yield for the Ru/Al_2O_3 hybrid- bed and Ni/Al_2O_3, respectively

Table 6. Parameters for the catalyst cost estimation

	Ru/Al_2O_3	Ni/Al_2O_3
Metal load (wt.%)	0.5 %	35 %
Relative mass for 99.5 % yield	1	1.89
Metal-Based		
Cost metal (€/kg)[1]	8233	12
Relative catalyst cost	5.20	1
Precursor based		
Cost metal in the precursor (€/kg_{met})[2]	207900	680
Relative catalyst cost	2.46	1
Commercial catalyst based		
Cost metal in the catalyst (€/kg_{met})[2]	592800	1700
Relative catalyst cost	2.64	1

Based on the simulation results, it is possible to perform the evaluation of the catalyst cost for the two different processes (Ru- and Ni-based). The parameters for the calculation are reported in Table 6. The catalyst cost was calculated according to the formula:

$$Cost\ \left(\frac{€}{reactor}\right) = metal\ load\ (wt.\%)\ \times\ metal\ content\ in\ precursor\ \left(\frac{wt.metal}{wt.tot}\right)\ \times\ cost\ precursor\ \left(\frac{€}{kg}\right)\ \times\ catalyst\ required\ \left(\frac{kg}{reactor}\right) \quad (23)$$

The two catalysts have a different metal load, which is 0.5 wt % for Ru/Al_2O_3 and 35% for Ni/Al_2O_3. We previously observed that the catalyst ratio to reach 99.5% yield of methane is ca. 1:2 in favour of Ru. However, Ru is a much more expensive metal than Ni. Currently, the price ratio of the two metals is 800:1. As a combination of these parameters, we observed that for the pure cost of the metal, the reactor operating with Ru/Al_2O_3 is 5.2 times more expensive than the equivalent reactor operating with Ni/Al_2O_3. However, the cost of the

[1] Data from http://www.infomine.com/investment/metal-prices/ruthenium/ (data recorded on 11.9.19)
[2] Data from Sigma-Aldrich

catalyst is not directly correlated to the cost of the pure metal. In fact, if we consider the catalyst cost on the base of different metal carrier substances, the comparison is substantially different. The cost of the metal in the form of precursor (Ru nitrosyl nitrate [36] and $Ni(NO_3)_2$ [10], respectively) is much higher than the pure metal cost, resulting in 25 times higher cost for Ru and 53 times higher for that of Ni. This difference causes a decrease in the relative cost of the two catalysts so that the precursor-based cost ratio is reduced to 2.46. If the comparison is made on the basis of the cost of the commercially available catalyst, the cost of the metals is further increased, with a cost ratio compared to the pure metal of 72 for Ru and 142 for Ni. In this case, the relative cost of the reactor bed is 2.64, in line with the precursor-based case. This means that the costs related to the preparation of the catalysts from the pure metals tend to decrease the price ratio of the final product. If the final price of the catalysts is considered, the cost of a Ru-based catalytic bed to perform the Sabatier reaction is ca. 2.5 times higher than the Ni bed with equivalent performance. However, apart from the pure catalyst cost, several other elements have to be considered for a detailed cost analysis of the entire process:

- The Ni-based catalysts are well-known to be prone to sintering. The maximal temperature that the Ni catalyst can withstand is limited to 575°C [25], while Ru is resistant at higher temperatures [37]. For this reason, the addition of steam in the feed stream is necessary [38]. This causes a decrease in the performance of the reactor due to the thermodynamic limitations (water is a product of the reaction). For example, if we use a CO_2/H_2O ratio of 0.5 in the feed [38], this leads to an increase of the volume of Ni required of 1.5 times, with a consequent decrease of the previously calculated cost ratio Ru/Ni to 1.67. This shows that a real reactor operating with Ni/Al_2O_3 has lower performance compared to the calculations shown in this work, requiring more catalyst than the amount computed herein.
- The process based on Ni/Al_2O_3 requires a condensation step, which brings additional capital costs related to the manufacturing and installation of the condenser, at least two additional heat exchangers and two separate reactive sections. This cost has to be evaluated in detail according to the specific size and application of the Sabatier reactor. The precise evaluation of this cost is however outside of the scope of this paper.

Given these considerations, we can conclude that Ru/Al_2O_3 is the preferred solution for small scale applications where heat integration is made more challenging and the compactness of the system is crucial. At larger scales, the greater complexity of the system could be economically sustainable after applying a scaling factor, and thus, the use of Ni-based catalysts may become beneficial.

4. Conclusions

The performance of Ru- and Ni-based catalysts for the Sabatier reaction is assessed based on various kinetic models. The key element for the operation of the reactor is the activity of the catalyst at temperatures below 300°C, to ensure the correct activation of the reactor and achievement of the high methane yield required for direct injection into the natural gas grid. The commercial Ru/Al_2O_3 catalyst is already active in the methanation reaction at 200°C, while the $Ni/Mg/Al_2O_4$ activates the reaction at 100°C higher. New tailor-made Ni-based catalysts can decrease this difference, but, as of today, the minimal activation temperature difference remains larger than 10-20 °C. Once the reaction is activated, the two reactors have approximately the same performance until a CO_2 conversion of ca. 85% is reached. This shows that both catalysts can reach the maximum allowed reaction rate in this part of the reaction. This is due to two phenomena: on the one hand, the reaction is dominated by the thermodynamic equilibrium, so that the reaction rate is controlled by cooling; on the other hand, however, Ru/Al_2O_3 is more subject to diffusion limitations at high temperature, resulting in a decrease in the observed reaction rate. The difference in the two reactive systems again becomes evident at high CO_2 conversions. Since the thermodynamic limitation requires low temperature, Ru/Al_2O_3 can reach 99.5% conversion without the need for an intermediate condensation step, while this conversion level is not attainable with the $Ni/Mg/Al_2O_4$ that is commercially used in steam reforming. The use of tailored Ni catalysts (such as a 35 wt.% Ni/Al_2O_3) can overcome this problem, reaching the desired conversion value with a single intermediate condensation stage. However, the amount of catalyst required is approximately double that of Ru/Al_2O_3. As the metal load in the Ni catalyst is two orders of magnitude higher than that of Ru, the calculated cost of a Ru-based catalytic bed is double that of Ni with the same performance. This means that, for

small-scale applications, where a simple reactive system is highly desirable, the use of Ru/Al_2O_3 could be beneficial compared to Ni-based systems.

This paper demonstrates that Ru/Al_2O_3 is the best reference catalyst for small-scale applications for the production of SNG. Recently developed catalysts have shown that the same performance as Ru/Al_2O_3 could be achieved with Ni-based catalysts, with one single intermediate condensation step. However, the high metal load of the latter systems reduces the benefit in using them as catalysts for the Sabatier reaction. For this reason, the focus of future research on this topic should be the decrease of the metal content in the catalysts, for example, by the addition of appropriate promoters.

Acknowledgements

The collaboration with Gaznat and the financial support from KTI/CTI (Innosuisse), project no. 26441.1 PFIW-IW “Development of a Novel, Highly Efficient Energy System for Natural Gas Metering and Regulating Stations Based on Waste Heat Recovery and Synthetic Methane Production”, are gratefully acknowledged.

Conflicts of interest

There are no conflicts of interest to declare.

References:

[1] J. Gao, Q. Liu, F. Gu, B. Liu, Z. Zhong, F. Su, Recent advances in methanation catalysts for the production of synthetic natural gas, RSC Adv. 5 (2015) 22759–22776. doi:10.1039/c4ra16114a.

[2] M. de Falco, G. Iaquaniello, G. Centi, CO2: A valuable source of carbon, 2013. doi:10.1007/978-1-4471-5119-7.

[3] A. Züttel, A. Remhof, A. Borgschulte, O. Friedrichs, Hydrogen: The future energy carrier, Philos. Trans. R. Soc. A Math. Phys. Eng. Sci. 368 (2010) 3329–3342. doi:10.1098/rsta.2010.0113.

[4] T. Schaaf, J. Grünig, M.R. Schuster, T. Rothenfluh, A. Orth, Methanation of CO2-storage of renewable energy in a gas distribution system, Energy. Sustain. Soc. 4 (2014) 1–14. doi:10.1186/s13705-014-0029-1.

[5] S. Rönsch, J. Schneider, S. Matthischke, M. Schlüter, M. Götz, J. Lefebvre, P. Prabhakaran, S. Bajohr, Review on methanation - From fundamentals to current projects, Fuel. 166 (2016) 276–296. doi:10.1016/j.fuel.2015.10.111.

[6] J.B. Sabatier, P., Senderes, Nouvelle synthèse du méthane, C. R. Acad. Sci. Paris. 134 (1902) 514–416.

[7] J. Gao, Y. Wang, Y. Ping, D. Hu, G. Xu, F. Gu, F. Su, A thermodynamic analysis of methanation reactions of carbon oxides for the production of synthetic natural gas, RSC Adv. 2 (2012) 2358–2368. doi:10.1039/C2RA00632D.
[8] G.A. Mills, F.W. Steffgen, Catalytic Methanation, Catal. Rev. 8 (1974) 159–210. doi:10.1080/01614947408071860.
[9] S. Abelló, C. Berrueco, D. Montané, High-loaded nickel – alumina catalyst for direct CO 2 hydrogenation into synthetic natural gas (SNG), 113 (2013) 598–609. doi:10.1016/j.fuel.2013.06.012.
[10] F. Koschany, D. Schlereth, O. Hinrichsen, On the kinetics of the methanation of carbon dioxide on coprecipitated NiAl (O) x, Appl. Catal. B, Environ. 181 (2016) 504–516. doi:10.1016/j.apcatb.2015.07.026.
[11] W.L. Vrijburg, E. Moioli, W. Chen, M. Zhang, B. Terlingen, B. Zijlstra, I.A.W. Filot, A. Zuttel, E.A. Pidko, E.J.M. Hensen, An Efficient Base-Metal NiMn/TiO2 Catalyst for CO2 Methanation, ACS Catal. (2019) acscatal.9b01968. doi:10.1021/acscatal.9b01968.
[12] I. Czekaj, F. Loviat, F. Raimondi, J. Wambach, S. Biollaz, A. Wokaun, Characterization of surface processes at the Ni-based catalyst during the methanation of biomass-derived synthesis gas: X-ray photoelectron spectroscopy (XPS), Appl. Catal. A Gen. 329 (2007) 68–78. doi:10.1016/j.apcata.2007.06.027.
[13] C. Mirodatos, H. Praliaud, M. Primet, Deactivation of nickel-based catalysts during CO methanation and disproportionation, J. Catal. 107 (1987) 275–287. doi:10.1016/0021-9517(87)90294-6.
[14] B. Miao, S.S.K. Ma, X. Wang, H. Su, S.H. Chan, Catalysis mechanisms of CO 2 and CO methanation, Catal. Sci. Technol. 6 (2016) 4048–4058. doi:10.1039/c6cy00478d.
[15] C. Janke, M.S. Duyar, M. Hoskins, R. Farrauto, Catalytic and adsorption studies for the hydrogenation of CO2 to methane, Appl. Catal. B Environ. 152–153 (2014) 184–191. doi:10.1016/j.apcatb.2014.01.016.
[16] J.H. Kwak, L. Kovarik, J. Szanyi, CO2 Reduction on Supported Ru/Al2O3 Catalysts: Cluster Size Dependence of Product Selectivity, ACS Catal. 3 (2013) 2449–2455. doi:10.1021/cs400381f.
[17] P. Panagiotopoulou, X.E. Verykios, Mechanistic Study of the Selective Methanation of CO over Ru/TiO2 Catalysts: Effect of Metal Crystallite Size on the Nature of Active Surface Species and Reaction Pathways, J. Phys. Chem. C. 121 (2017) 5058–5068. doi:10.1021/acs.jpcc.6b12091.
[18] M. Marwood, R. Doepper, M. Prairie, A. Renken, Transient drift spectroscopy for the determination of the surface reaction kinetics of CO2 methanation, Chem. Eng. Sci. 49 (1994) 4801–4809. doi:10.1016/S0009-2509(05)80060-0.
[19] S. Sharma, Z. Hu, P. Zhang, E.W. McFarland, H. Metiu, CO2 methanation on Ru-doped ceria, J. Catal. 278 (2011) 297–309. doi:10.1016/j.jcat.2010.12.015.
[20] D.C. Upham, A.R. Derk, S. Sharma, H. Metiu, E.W. McFarland, CO2 methanation by Ru-doped ceria: The role of the oxidation state of the surface, Catal. Sci. Technol. 5 (2015) 1783–1791. doi:10.1039/c4cy01106f.
[21] A. Moioli, Emanuele; Gallandat, Noris; Züttel, Model based determination of the optimal reactor concept for Sabatier reaction in small-scale applications over Ru/Al2O3, Chem. Eng. J. 375 (2019) 121954. doi:10.1016/j.cej.2019.121954.
[22] M.A.A. Aziz, A.A. Jalil, S. Triwahyono, A. Ahmad, CO2 methanation over heterogeneous catalysts: Recent progress and future prospects, Green Chem. 17 (2015) 2647–2663. doi:10.1039/c5gc00119f.

[23] J.M.G. Carballo, E. Finocchio, S. García-Rodriguez, M. Ojeda, J.L.G. Fierro, G. Busca, S. Rojas, Insights into the deactivation and reactivation of Ru/TiO 2 during Fischer-Tropsch synthesis, Catal. Today. 214 (2013) 2–11. doi:10.1016/j.cattod.2012.09.018.
[24] L. Falbo, M. Martinelli, C.G. Visconti, L. Lietti, C. Bassano, P. Deiana, Kinetics of CO2methanation on a Ru-based catalyst at process conditions relevant for Power-to-Gas applications, Appl. Catal. B Environ. 225 (2018) 354–363. doi:10.1016/j.apcatb.2017.11.066.
[25] J.G. Xu, G.F. Froment, Methane Steam Reforming, Methanation and Water-Gas Shift .1. Intrinsic Kinetics, Aiche J. 35 (1989) 88–96. doi:10.1002/aic.690350109.
[26] J.A.H. Dreyer, P. Li, L. Zhang, G.K. Beh, R. Zhang, P.H.L. Sit, W.Y. Teoh, Influence of the oxide support reducibility on the CO2methanation over Ru-based catalysts, Appl. Catal. B Environ. 219 (2017) 715–726. doi:10.1016/j.apcatb.2017.08.011.
[27] R. Mutschler, E. Moioli, W. Luo, N. Gallandat, A. Züttel, CO2hydrogenation reaction over pristine Fe, Co, Ni, Cu and Al2O3supported Ru: Comparison and determination of the activation energies, J. Catal. 366 (2018) 139–149. doi:10.1016/j.jcat.2018.08.002.
[28] A. Porta, L. Falbo, C. Giorgio, L. Lietti, C. Bassano, P. Deiana, Synthesis of Ru-based catalysts for CO 2 methanation and experimental assessment of intraporous transport limitations, Catal. Today. (2019). doi:10.1016/j.cattod.2019.01.042.
[29] G. F. Froment, Classification of Fixed Bed Reactor Models, Anal. Des. Fixed Bed Catal. React. 109 (1974). http://pubs.acs.org.
[30] A.P. de Wasch, G.F. Froment, Heat transfer in packed beds, Chem. Eng. Sci. 27 (1972) 567–576. doi:10.1016/0009-2509(72)87012-X.
[31] L.M. Aparicio, Transient isotopic studies and microkinetic modeling of methane reforming over nickel catalysts, J. Catal. 165 (1997) 262–274. doi:10.1006/jcat.1997.1468.
[32] D. Schlereth, O. Hinrichsen, A fixed-bed reactor modeling study on the methanation of CO2, Chem. Eng. Res. Des. 92 (2014) 702–712. doi:10.1016/j.cherd.2013.11.014.
[33] E. Tsotsas, Wärmeleitung und Dispersion in durchströmten Schüttungen, (2018) 1–20. doi:10.1007/978-3-662-52991-1_102-1.
[34] N. Wakao, S. Kaguei, T. Funazkri, Effect of fluid dispersion coefficients on particle-to-fluid heat transfer coefficients in packed beds. Correlation of nusselt numbers, Chem. Eng. Sci. 34 (1979) 325–336. doi:10.1016/0009-2509(79)85064-2.
[35] E. Moioli, N. Gallandat, A. Züttel, Parametric sensitivity in the Sabatier reaction over Ru/Al2O3 – theoretical determination of the minimal requirements for reactor activation, React. Chem. Eng. 4 (2019) 100–111. doi:10.1039/C8RE00133B.
[36] L. Falbo, M. Martinelli, C.G. Visconti, L. Lietti, C. Bassano, P. Deiana, Kinetics of CO2methanation on a Ru-based catalyst at process conditions relevant for Power-to-Gas applications, Appl. Catal. B Environ. 225 (2018) 354–363. doi:10.1016/j.apcatb.2017.11.066.
[37] N. Gallandat, R. Mutschler, V. Vernay, H. Yang, A. Züttel, Experimental performance investigation of a 2 kW methanation reactor, Sustain. Energy Fuels. 2 (2018) 1101–1110. doi:10.1039/C8SE00073E.
[38] J. Witte, J. Settino, S.M.A. Biollaz, T.J. Schildhauer, Direct catalytic methanation of biogas – Part II: Techno-economic process assessment and feasibility reflections, Energy Convers. Manag. 178 (2018) 26–43. doi:10.1016/j.enconman.2018.05.056.